

Analyses of Coronavirus Assembly Interactions with Interspecies Membrane and Nucleocapsid Protein Chimeras

Lili Kuo, Kelley R. Hurst-Hess, Cheri A. Koetzner, Paul S. Masters

Wadsworth Center, New York State Department of Health, Albany, New York, USA

ABSTRACT

The coronavirus membrane (M) protein is the central actor in virion morphogenesis. M organizes the components of the viral membrane, and interactions of M with itself and with the nucleocapsid (N) protein drive virus assembly and budding. In order to further define M-M and M-N interactions, we constructed mutants of the model coronavirus mouse hepatitis virus (MHV) in which all or part of the M protein was replaced by its phylogenetically divergent counterpart from severe acute respiratory syndrome coronavirus (SARS-CoV). We were able to obtain viable chimeras containing the entire SARS-CoV M protein as well as mutants with intramolecular substitutions that partitioned M protein at the boundaries between the ectodomain, transmembrane domains, or endodomain. Our results show that the carboxy-terminal domain of N protein, N3, is necessary and sufficient for interaction with M protein. However, despite some previous genetic and biochemical evidence that mapped interactions with N to the carboxy terminus of M, it was not possible to define a short linear region of M protein sufficient for assembly with N. Thus, interactions with N protein likely involve multiple linearly discontinuous regions of the M endodomain. The SARS-CoV M chimera exhibited a conditional growth defect that was partially suppressed by mutations in the envelope (E) protein. Moreover, virions of the M chimera were markedly deficient in spike (S) protein incorporation. These findings suggest that the interactions of M protein with both E and S protein are more complex than previously thought.

IMPORTANCE

The assembly of coronavirus virions entails concerted interactions among the viral structural proteins and the RNA genome. One strategy to study this process is through construction of interspecies chimeras that preserve or disrupt particular inter- or intramolecular associations. In this work, we replaced the membrane (M) protein of the model coronavirus mouse hepatitis virus with its counterpart from a heterologous coronavirus. The results clarify our understanding of the interaction between the coronavirus M protein and the nucleocapsid protein. At the same time, they reveal unanticipated complexities in the interactions of M with the viral spike and envelope proteins.

Coronaviruses (CoVs) are a family of enveloped positive-strand RNA viruses that cause disease in numerous mammalian and avian hosts (1, 2). Of the six coronaviruses that can infect humans, the two of greatest current concern are the etiologic agents of severe acute respiratory syndrome (SARS-CoV) and Middle East respiratory syndrome (MERS-CoV). Virions of coronaviruses contain a canonical set of four structural proteins. The most numerous constituent, the membrane (M) protein, makes up a lattice in the viral envelope that associates with the other components. Trimers of spike (S) protein form projections on the virion surface responsible for attachment to host cell receptors, and minor amounts of the small envelope (E) protein also appear in the viral membrane. In the virion interior, the nucleocapsid (N) protein encloses the ~30-kb viral genome into a helically symmetric ribonucleoprotein.

Much of our knowledge of coronavirus assembly has been worked out through studies with the prototype coronavirus mouse hepatitis virus (MHV). MHV falls into the betacoronaviruses, the second of the four genera of the family and the one which also includes SARS-CoV and MERS-CoV. Key contributions to understanding virion morphogenesis have also been made through analyses of the gammacoronavirus infectious bronchitis virus (IBV) and the alphacoronavirus transmissible gastroenteritis virus (TGEV). A large body of work points to M protein as the major player in virion assembly. Coexpression of subsets of viral proteins revealed that just M protein and E protein are suffi-

cient for the formation of virus-like particles (VLPs) (3–5). The inclusion of N protein, although it is not strictly required, greatly enhances the efficiency of VLP formation (6, 7). The critical role of E protein is carried out at the site of budding, the endoplasmic reticulum-Golgi intermediate compartment, with very little E being carried over into assembled virions (8). Additionally, M protein captures S protein for incorporation into virions or VLPs (9, 10), but S is an optional participant in virus formation (11, 12), even though it is essential for infectivity.

Thus, extensive networks of protein-protein interactions in coronavirus assembly involve one or both of the most abundant virion components, M and N. The N protein is a highly basic phosphoprotein containing the structurally distinct amino-terminal RNA-binding domain (NTD) and the carboxy-terminal RNA-binding domain (CTD) (13), which we have previously called domains N1b and N2b, respectively (14–16) (Fig. 1A). In MHV N

Received 22 December 2015 Accepted 8 February 2016

Accepted manuscript posted online 17 February 2016

Citation Kuo L, Hurst-Hess KR, Koetzner CA, Masters PS. 2016. Analyses of coronavirus assembly interactions with interspecies membrane and nucleocapsid protein chimeras. *J Virol* 90:4357–4368. doi:10.1128/JVI.03212-15.

Editor: S. Perlman

Address correspondence to Paul S. Masters, Paul.Masters@health.ny.gov.

Copyright © 2016, American Society for Microbiology. All Rights Reserved.

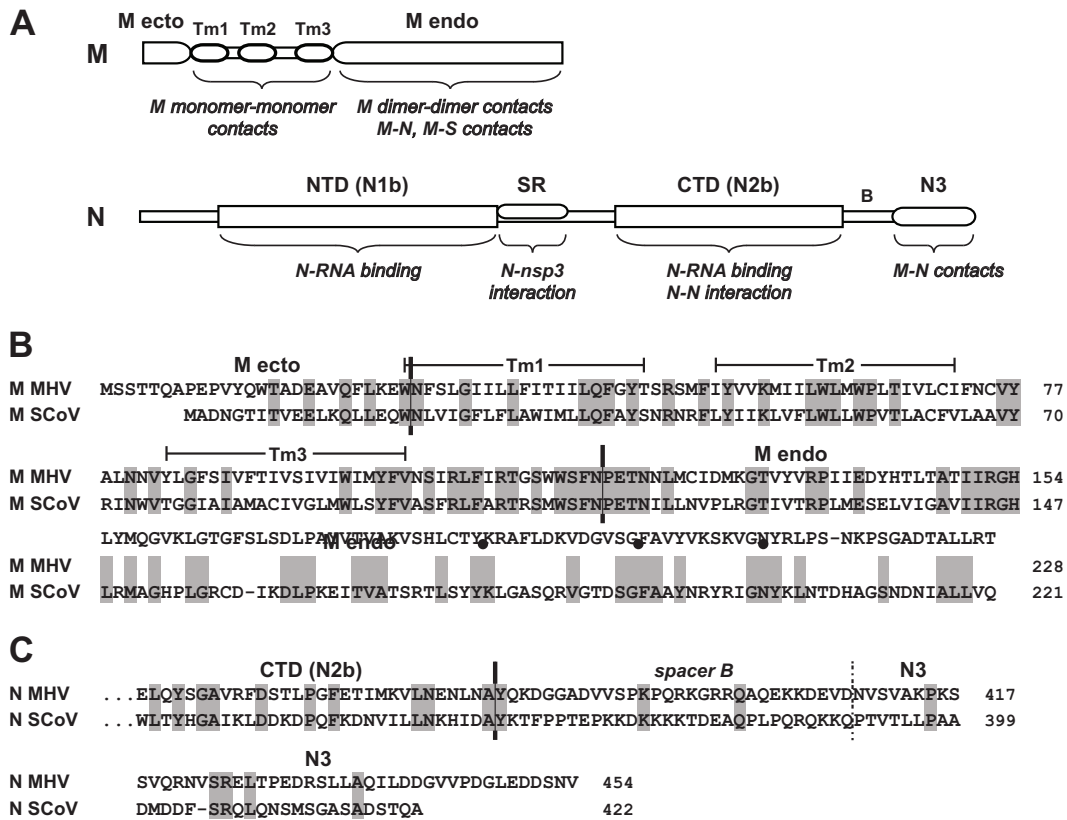


FIG 1 Coronavirus M- and N-protein domain structure. (A) Schematics of the M and N proteins with a summary of currently assigned interactions. Tm, transmembrane domain; NTD (N1b), amino-terminal RNA-binding domain; SR, serine- and arginine-rich region; CTD (N2b), carboxy-terminal RNA-binding domain; B, spacer region; N3, carboxy-terminal domain. (B) Alignment of the MHV and SARS-CoV (SCoV) M proteins. Tm domains are as modeled in the work of Rottier et al. (29). Vertical bars between the ectodomain (ecto), Tm domains, and endodomain (endo), functional crossover boundaries in the constructed chimeras; filled circles, nonfunctional crossover boundaries within the M endodomain. (C) Alignment of the carboxy termini of the MHV and SARS-CoV N proteins. Vertical bar, the functional crossover boundary in chimeras; broken line, boundary between spacer B and domain N3. The GenBank accession numbers for the sequences shown are [AY700211](#) for MHV A59 and [AY278741](#) for SARS-CoV strain Urbani.

protein, the CTD, but not the NTD, is a critical determinant for recognition of the genomic RNA packaging signal (16). The CTD also mediates N-N dimerization and longer-range interactions in the nucleocapsid (17). Flanking the NTD and CTD are intrinsically disordered protein segments (13, 18). One of these, the linker between the NTD and CTD, harbors a serine- and arginine-rich (SR) region that binds to the replicase nonstructural protein 3 (nsp3) in an interaction crucial to an early step of infection (15, 19). At the carboxy terminus of the molecule is domain N3, which many (20–24), but not all (25–27), prior studies have assigned to be the locus of N-M interactions.

The M protein is a triple-spanning transmembrane protein with a small ectodomain and a large carboxy-terminal endodomain (28, 29) (Fig. 1A). As yet, there is only limited structural information available for M. The assignment of intra- and intermolecular interactions to parts of the M protein is more tentative than that to parts of the N protein. Evidence from cryo-electron micrographic (cryo-EM) and tomographic reconstructions (30) and inferences drawn from a genetic study of evolved M mutants (31) suggest that M-M monomer interactions occur among the transmembrane (Tm) domains, whereas higher-order oligomerization of M dimers is governed by the endodomain. The endodomain is also the locus of interactions of M protein with N protein

(20–24, 32, 33) and with S protein (34, 35). In order to learn more about the intra- and intermolecular interactions of M, we constructed MHV chimeras containing entire or partial substitutions of the SARS-CoV M protein. This strategy allowed us to further define M-N and M-M interactions. Additionally, it revealed that the interactions of M with the E and S proteins are more complex than currently pictured.

MATERIALS AND METHODS

Cells and viruses. MHV A59 wild-type and mutant virus stocks were grown at 37°C in mouse 17 clone 1 (17C11) cells. Plaque titrations and plaque purifications were performed with mouse L2 cells. The host-range chimeric coronavirus designated fMHV.v2 (36), used as the recipient virus for reverse genetics, was grown in feline FCWF cells.

MHV mutant construction. All mutants in this study were isolated by targeted RNA recombination, as previously described in detail (36, 37). Transcription vectors for donor RNA synthesis were constructed from plasmid pSG6X (16), which contains the 3′-most 8.6 kb of the MHV A59 genome. To create vector pMN1, SARS-CoV domain N3 was transferred to pSG6X from the previously described pMN54-SN3 (15) by transfer of the NheI-BstEII fragment, which runs from the center of the N gene through the start of the 3′ untranslated region. All subsequent constructs containing SARS-CoV domain N3 were then derived from pMN1. Whole or partial SARS-CoV M-gene substitutions were made through manipu-

lation of the EcoRV-PspXI fragment running from the end of the E gene through the M gene and to the start of the N gene. Chimeric sequences were generated via PCR or two-step PCR using a cloned SARS-CoV M-gene cDNA as the template (strain Urbani; GenBank accession number [AY278741](#)). Alternatively, some M-gene fragments were synthesized by PCR from overlapping oligonucleotides and inserted into plasmids using the EagI or BssHII site within M or a coding-silent BspEI site that was created at MHV M codons 198 and 199 (equivalent to SARS-CoV M codons 190 and 191, respectively). The entire SARS-CoV M substitution in vectors pMN2, pMN3, pMN6, and pMN7 was an exact replacement of the MHV M open reading frame (ORF). The junctions in the partial SARS-CoV M substitutions in vectors pMN4A, pMN4B, pMN4C, pMN5A, pMN5B, pMN8, pMN9, and pMN10 were made at the various boundaries shown in [Fig. 1B](#). The SARS-CoV E gene in vector pMN6, which is an exact ORF-for-ORF replacement, was obtained by transfer from the previously described pLK106 ([38](#)) of the SbfI-EcoRV fragment, which runs from immediately downstream of the S gene through the end of the E gene. Similarly, the E-gene F20S mutation was placed in vectors pMN5A, pMN5B, pMN7, pMN8, and pMN10 by transfer of an SbfI-EcoRV fragment of cDNA from mutant MN3rev3. Oligonucleotides for PCR and DNA sequencing were obtained from Integrated DNA Technologies. The overall compositions of the constructed plasmids were confirmed by restriction analysis, and all ligation junctions and regions generated by PCR amplification were verified by DNA sequencing.

The wild-type virus used in this work was Alb741, a recombinant that was previously isolated by targeted RNA recombination with donor RNA from pSG6X ([16](#)). For viable chimeric viral mutants, at least three independent isolates were obtained. In each case, once it was established in preliminary experiments that multiple isolates behaved identically, one of them was chosen for further analysis. The exceptions were mutants MN6 and MN7, each of which was isolated only once. Particular chimeric constructs were judged to be lethal after yielding no recombinants in multiple targeted RNA recombination experiments for which parallel positive controls with wild-type donor RNA produced recombinants at a robust frequency.

Virus purification. The wild-type and mutant MN8 viruses were grown in 17C11 cell monolayers infected at a multiplicity of 1 PFU/cell. Medium containing released virus was harvested at 14 h postinfection, at a point when the monolayers exhibited maximal syncytium formation but minimal lysis or detachment. Virions were purified by polyethylene glycol precipitation followed by equilibrium centrifugation on preformed gradients of 20 to 30% iodixanol (OptiPrep; Sigma-Aldrich) in a buffer of 50 mM Tris-maleate (pH 6.5) and 1 mM EDTA. Gradients were centrifuged at $111,000 \times g$ in a Beckman SW41 rotor at 4°C for 18 h, and for each gradient, 15 750- μ l fractions were collected from the top.

Northern blotting. RNA was extracted from aliquots of the gradient fractions with the TRI Reagent (Zymo) according to the manufacturer's instructions. Purified RNA denatured with formaldehyde and formamide was directly dot blotted onto Nytran Supercharge membranes (Whatman; GE Healthcare) by filtration through a vacuum manifold, followed by UV cross-linking. Membranes were hybridized with a PCR-amplified probe corresponding to nucleotides 401 to 909 of the MHV genome, a region unique to genomic RNA (and absent from subgenomic RNA). The probe was labeled by use of an AlkPhos Direct kit; the RNA in the blots was visualized using the CDP-Star detection reagent (GE Healthcare) and quantitated with a Bio-Rad ChemiDoc XRS+ instrument.

Western blotting. Purified virions or NP-40 lysates prepared from infected 17C11 cell monolayers were separated by sodium dodecyl sulfate-polyacrylamide gel electrophoresis (SDS-PAGE; 10%, except where indicated otherwise) and analyzed by Western blotting exactly as described previously ([31](#)). Proteins were detected with one of the following: anti-MHV N-protein rabbit polyclonal antibody ([14](#)); anti-MHV M-protein monoclonal antibody J.1.3, generously provided by John Fleming, University of Wisconsin, Madison, WI; anti-SARS-CoV M-protein monoclonal antibody NR-621, similar to 283C ([39](#)), obtained through the NIH

Biodefense and Emerging Infections Research Resources Repository; or anti-MHV S-protein rabbit polyclonal antibody raised against a peptide corresponding to the carboxy-terminal 13 residues of S (DSIVIHNISSHED). Bound antibodies were visualized by enhanced chemiluminescence detection (Pierce), and quantitation was carried out with a Bio-Rad ChemiDoc XRS+ instrument.

RESULTS

Construction of an MHV mutant containing the entire SARS-CoV M protein. To more completely elucidate the structural protein requirements for coronavirus assembly, we constructed an MHV chimera containing the SARS-CoV M protein. The equivalence of the M endodomain of MHV with that of the very closely related bovine coronavirus (BCoV) was demonstrated in an earlier study ([40](#)). However, we anticipated that substitution of the much less homologous SARS-CoV M protein would provide a more stringent test of compatible and incompatible intermolecular interactions. The M proteins of MHV and SARS-CoV, which are lineage A and lineage B betacoronaviruses, respectively, share only 38% amino acid sequence identity ([Fig. 1B](#)). Although M protein is known to engage with each of the other three coronavirus structural proteins, we did not expect that a SARS-CoV M chimera would be significantly hindered in essential M-S or M-E interactions. We had previously found that the SARS-CoV E protein could functionally substitute for the MHV E protein ([38](#)). Additionally, it was shown that the endodomain of the MHV S protein, the region of S that interacts with M ([41, 42](#)), could be completely replaced by its SARS-CoV counterpart ([43](#)).

In contrast, we postulated that substitution of a heterologous M protein would require that it be partnered with the region of N protein that assembles with M. Much prior work indicated that N interactions with M are confined to the carboxy-terminal domain of N protein (domain N3) ([20–24](#)), which has little or no sequence homology between MHV and SARS-CoV ([Fig. 1C](#)). Accordingly, we used targeted RNA recombination ([36, 37](#)) to isolate an MHV mutant, MN3, which harbored the complete SARS-CoV M protein as well as domain N3 (plus the adjacent spacer B) of SARS-CoV N protein ([Fig. 2A](#)). Consistent with our initial assumptions, a chimeric construct that paired the MHV M protein with the SARS-CoV domain N3 (mutant MN1) was lethal, confirming earlier results ([15](#)). Likewise, a chimeric construct that paired the SARS-CoV M protein with the MHV domain N3 (mutant MN2) was also lethal. These results showed that domain N3 is essential for the functional interaction between the coronavirus N and M proteins. Previous work has established that the highly variable spacer B is not essential for virion formation. MHV N spacer B can be altered with a divergent coronavirus sequence ([44](#)) or an epitope tag ([21](#)) or even entirely replaced with a synthetic flexible linker peptide sequence ([14](#)). Moreover, the complete deletion of spacer B in the classical temperature-sensitive mutant Alb4 still allows virion assembly at the permissive temperature ([45](#)).

Three independent isolates of the MN3 mutant were obtained, and their sequences were confirmed. Two of the three contained the exact SARS-CoV M-gene sequence. The third isolate had two coding changes in M, N206S and T207A. However, since this virus was phenotypically identical to the other two, these mutations were deemed extraneous, and one (unmutated) isolate was chosen for further study. Notably, none of the MN3 isolates had any sequence changes in the S endodomain, the E gene, or the chimeric N gene. Thus, the substitution of the SARS-CoV M protein did not

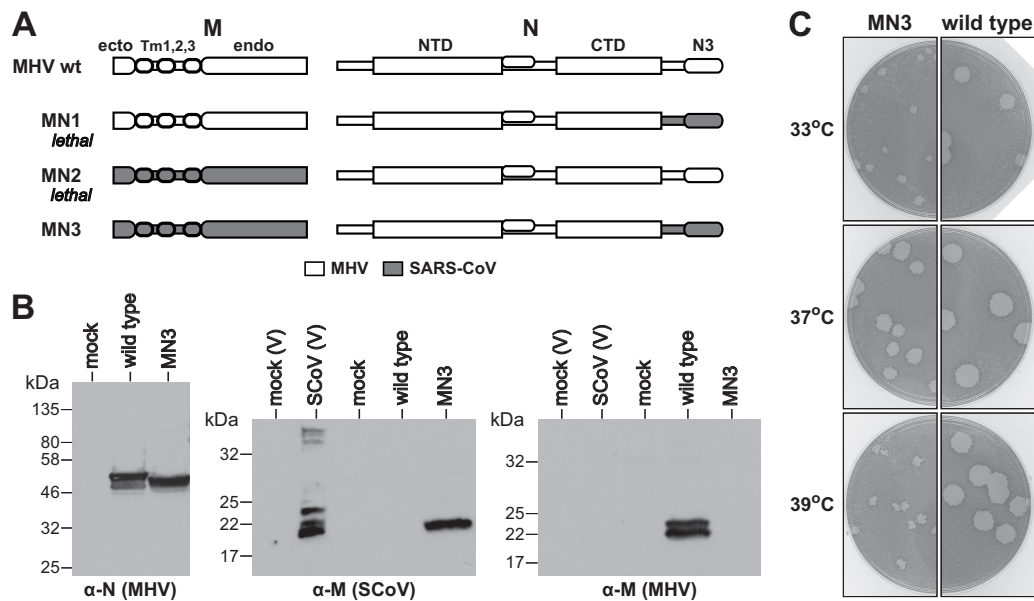


FIG 2 Construction of an MHV chimera containing the entire M protein of SARS-CoV. (A) Schematics of wild-type (wt) virus and chimeras MN1, MN2, and MN3 containing mutant M and N proteins. Shading represents the sequence of SARS-CoV substituted for that of MHV. (B) Western blots of lysates from mouse 17C11 cells infected with wild-type MHV or MN3 virus; mock, uninfected 17C11 cells. Additional controls, designated mock (V) and SCoV (V), were protein fractions from TRIzol extracts of mock-infected and SARS-CoV-infected Vero cells, respectively. Blots were probed with polyclonal anti-MHV N antibody (left), monoclonal anti-SARS-CoV M antibody (middle), or monoclonal anti-MHV M antibody (right). (C) Plaques of the MN3 mutant (passage 2 stock) at 33, 37, or 39°C compared with those of the isogenic wild-type virus (passage 3 stock). Plaque titrations were carried out on L2 cells; monolayers were stained with neutral red at 72 h postinfection and were photographed 18 h later. Infectious titers measured at all three temperatures were 8.6×10^7 PFU/ml for the wild type and 2.3×10^6 PFU/ml for MN3.

depend upon the acquisition of second-site mutations in protein domains that interact with M protein, other than N3. To verify expression of proteins encoded by the chimeric virus, lysates from infected cells were analyzed by Western blotting (Fig. 2B). As expected, an anti-SARS-CoV M monoclonal antibody reacted with MN3 M protein but not with wild-type MHV M protein. Conversely, an anti-MHV M monoclonal antibody reacted with wild-type MHV M protein but not with MN3 M protein. Since the two anti-M antibodies recognize different epitopes, the level of M expression by MN3 could not be directly compared to that of the wild type. However, both viruses expressed comparable amounts of wild-type (49.7-kDa) or chimeric (48.3-kDa) N protein, as judged by probing infected cell lysates with polyclonal anti-MHV N antibody. Additionally, as predicted, a monoclonal antibody that recognizes an epitope in wild-type MHV domain N3 (21) did not react with the chimeric MN3 N protein (data not shown).

Although the MN3 mutant was viable, it grew to an ~40-fold lower infectious titer than did wild-type virus and formed smaller plaques at 37°C (Fig. 2C). This plaque size difference was more pronounced at 33°C, and at 39°C MN3 plaques were tiny compared to those of the wild type. This indicated that at least one of the intermolecular interactions of SARS-CoV M protein with MHV components was partially impaired.

Analysis of revertants of MN3. To gain an understanding of the defect in the SARS-CoV M chimera, we isolated mutants with improved growth following 6 to 10 serial passages at 39°C of multiple individual cultures of MN3, each of which had been started from a single plaque. These mutants (referred to as revertants here) formed plaques at 39°C that were markedly larger than those of the MN3 parent but that were not fully as large as wild-type

plaques. We mapped the mutations that had arisen in each by sequencing the S endodomain and the entire E, M, and N genes. Among 10 independent revertants that were isolated, 7 had single changes in the E protein, which localized in either the Tm domain or the endodomain (Fig. 3A). Of the three other revertants, two had mutations in SARS-CoV M (V96L or S172P) and one had a mutation in both S (H1310Y) and N (E146Q). Since most of the reverting mutations fell in E and since these were in the revertants which formed the largest plaques, this suggested that wild-type MHV E cannot optimally cooperate with SARS-CoV M in virion morphogenesis. Such a finding was unexpected, because we had previously found that the SARS-CoV E protein was nearly completely able to replace the MHV E protein (38).

More surprising was the finding that substitution of the entire SARS-CoV E protein in conjunction with the SARS-CoV M protein generated a virus whose fitness was further impaired, rather than improved, with respect to that of MN3. The resulting E-M chimera, MN6, formed very small plaques at 37°C and pinpoint plaques at 39°C (Fig. 3B and C), and it had an ~3-fold lower infectious titer. This unforeseen outcome may have been the consequence of distinct activities of the substituted E protein (46) acting in conflict with each other (see Discussion). To ascertain whether alteration of the MHV E protein was sufficient to enhance the fitness of the SARS-CoV M chimera, we reconstructed the mutation from the most robust of the revertants, MN3rev3. The MN7 construct, containing F20S in its E protein, exhibited substantially larger plaques than the MN3 mutant at both 37°C and 39°C (Fig. 3B and C), and it had a 20- to 30-fold higher infectious titer than MN3. This established that the F20S mutation alone is capable of significantly enhancing the growth of the MN3 mutant,

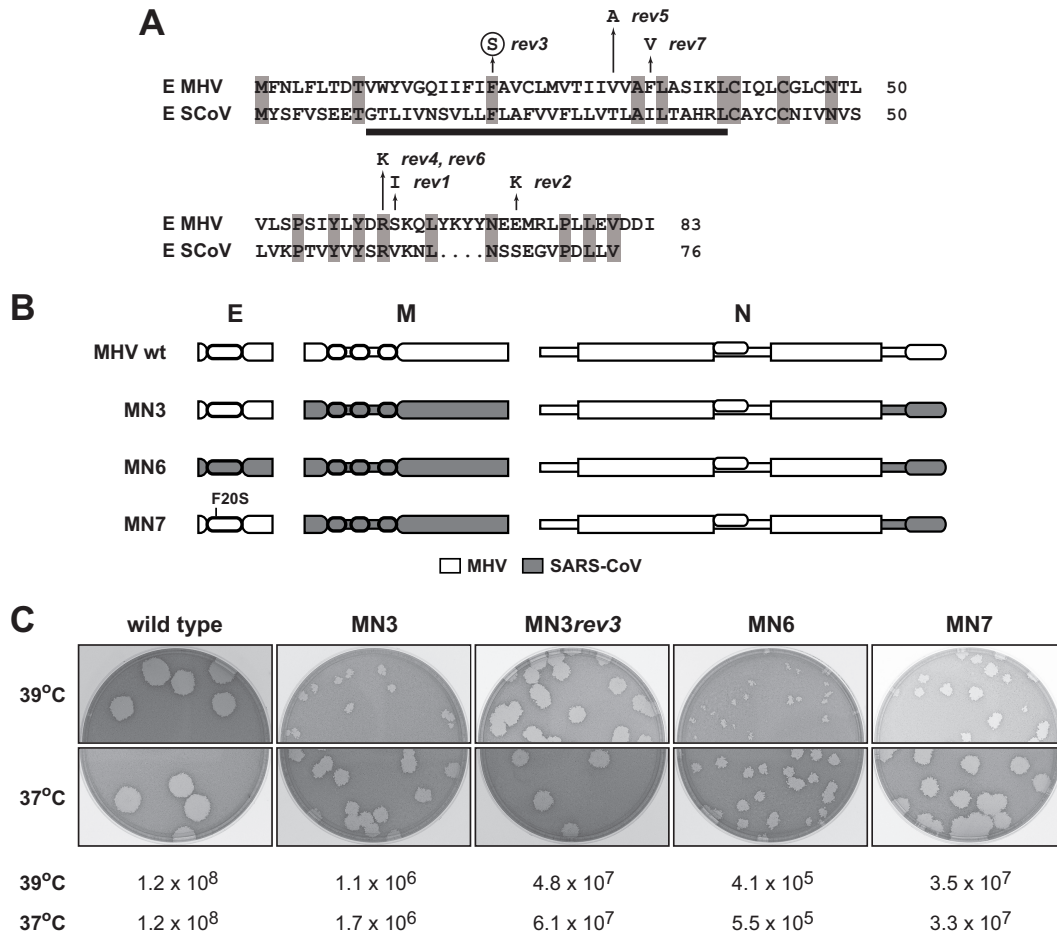


FIG 3 Effect of E-protein mutations on SARS-CoV M chimeras. (A) Alignment of MHV and SARS-CoV E proteins showing independent reverting mutations that enhance the growth of the MN3 chimera at 39°C. Solid bar, the Tm domain; the circled mutation of MN3rev3 (F20S), the mutation chosen for incorporation into subsequent constructs. The GenBank accession numbers for the sequences shown are [AY700211](#) for MHV A59 and [AY278741](#) for SARS-CoV strain Urbani. (B) Schematics of wild-type virus and chimeras containing mutant E, M, and N proteins. Shading represents the sequence of SARS-CoV substituted for that of MHV. (C) Plaques of wild-type, MN3, MN3rev3, MN6, and MN7 viruses at 37 and 39°C (passage 4 stock for the wild type, passage 2 stocks for the mutants). Plaque titrations were carried out on L2 cells; monolayers were stained with neutral red at 72 h postinfection and were photographed 18 h later. The infectious titers (numbers of PFU per milliliter) measured at each temperature are indicated.

suggesting that there exists an interaction between the E and M proteins. However, as MN7 did not entirely recapitulate the phenotype of MN3rev3, we determined the entire genomic sequence of the latter. This revealed four additional mutations in MN3rev3: D42G in nsp2, T298I in nsp15, S163L in the HE pseudogene, and F270V in the S-protein ectodomain. We think it likely that none of these points to a previously unknown interaction with M protein, although the S ectodomain mutation conceivably contributed to the larger plaque size of MN3rev3. We therefore included just the E protein F20S mutation in further M chimeric constructs.

Domain substitutions within the M protein. Multiple lines of evidence from previous structural (30), genetic (31), and virus-like particle (47) studies all suggest that the M-protein ectodomain, Tm domains, and endodomain might have separable roles in assembly. To test this notion, we generated intramolecular M-protein chimeric substitutions. The first of these, MN8 (Fig. 4A), retained the entire SARS-CoV M protein, except for the restoration of the MHV M ectodomain. The crossover point between the MHV and SARS-CoV sequences chosen was a conserved pair of

residues (WN) at the junction of the ectodomain and the first Tm domain (Fig. 1B). As with the MN7 construct, the E protein of MN8 incorporated the F20S mutation and domain N3 of the SARS-CoV N protein. In two additional recombinants, MN9 and MN10 (Fig. 4A), both the MHV ectodomain and Tm domains were restored to the SARS-CoV M protein. In this case, the constructed crossover between the MHV and SARS-CoV sequences was a motif (WSFNPETN) occurring shortly after the third Tm domain (Fig. 1B). This motif is highly conserved among all beta-coronavirus M proteins, and in MHV it has been shown to be critical for virus-like particle assembly and for virus viability (48). Mutant MN9 was made with the wild-type MHV E protein, while MN10 had the E-protein F20S mutation.

The ectodomains of the MHV and SARS-CoV M proteins diverge extensively (Fig. 1B). Moreover, the MHV-A59 M-protein ectodomain is O-glycosylated (49), whereas the SARS-CoV M-protein ectodomain is N-glycosylated (50). These differences appeared to have no major effect on the growth of MN8 at 37°C (Fig. 4B) relative to that previously seen for the complete SARS-CoV M

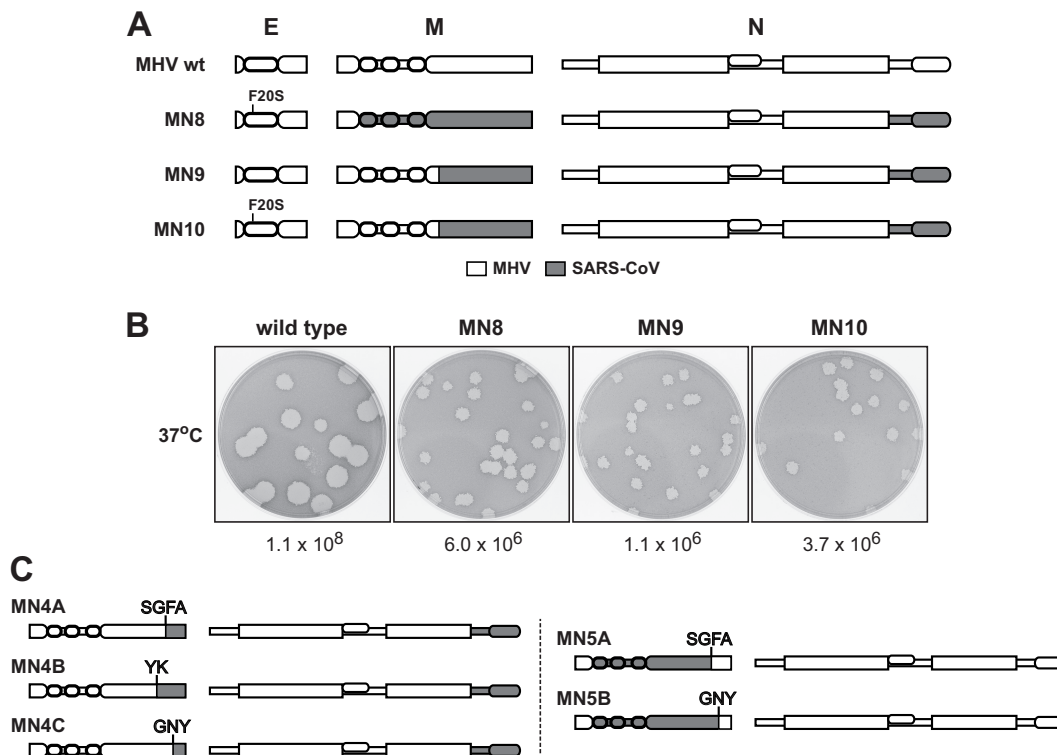


FIG 4 Intramolecular M-protein chimeric substitutions. (A) Schematics of wild-type virus and chimeras MN8, MN9, and MN10 containing mutant E, M, and N proteins. Shading represents the sequence of SARS-CoV substituted for that of MHV. (B) Plaques of wild-type, MN8, MN9, and MN10 viruses at 37°C (passage 4 stock for the wild type, passage 3 stocks for the mutants). Plaque titrations were carried out on L2 cells; monolayers were stained with neutral red at 72 h postinfection and were photographed 18 h later. The infectious titers (numbers of PFU per milliliter) measured are indicated. (C) Schematics of lethal substitutions in chimeras MN4A to MN4C, MN5A, and MN5B, made in attempts to define a carboxy-terminal subregion of the M endodomain sufficient for interaction with domain N3. MN5A and MN5B also contained the MHV E-gene mutation F20S.

substitution mutants MN3 and MN7. Likewise, the MN9 and MN10 mutants tolerated the pairing of heterologous Tm domains and endodomains within the M molecule, indicating that these two regions participate largely independently in intermolecular interactions. Nevertheless, it was noted that at 39°C all three mutants formed smaller plaques than did MN3 or MN7 (data not shown). This impairment was most profound for MN9, suggesting that in MN8 and MN10 the E-protein F20S mutation made a beneficial contribution to SARS-CoV M endodomain associations in M-protein oligomers.

In contrast to the substitutions that were allowed in MN8, MN9, and MN10, we were not able to subdivide the M-protein endodomain in order to define a minimal region capable of interacting with N protein. On the basis of prior evidence that the M-N interaction maps to the carboxy terminus of the M endodomain (20, 21, 23, 32), various potential crossover points between the two species of M protein were tested. In constructs MN4A, MN4B, and MN4C, the SARS-CoV sequence was grafted onto the tail of the MHV M protein at conserved residues positioned 30 (SGFA), 43 (YK), or 20 (GNY) amino acids, respectively, from the carboxy terminus (Fig. 1B and 4C). Reciprocal substitutions of the MHV M sequence on a SARS-CoV M background were also made in constructs MN5A and MN5B. In each case, domain N3 of the N protein was derived from the species to which the tail of the M protein belonged. None of these five constructs yielded viable viruses, despite numerous independent trials of targeted RNA recombination, some of which included mutagenized donor RNAs

and all of which had robust wild-type controls. The lethality of all of these mutants likely means that, due to the globular nature of the M endodomain, the surface that interacts with domain N3 is more complex than merely a linear stretch of primary sequence.

Analysis of virions of the SARS-CoV M-protein chimera. We consistently noted that monolayers inoculated with MN3 or MN8 at 37°C exhibited a progression of syncytium formation and cytopathic effect similar to that exhibited by monolayers inoculated with wild-type virus at the same multiplicity of infection. However, virus released from cells infected with either of these SARS-CoV M chimeras had a markedly lower infectious titer than the wild type. Moreover, preliminary evidence showed that virions of MN3 and MN8 were defective in the selective packaging of genomic RNA (L. Kuo and P. S. Masters, unpublished data), suggesting a possible basis for their reduced infectivity. These observations prompted us to examine SARS-CoV M chimeric virions in more detail. We chose MN8 for this analysis because its composition allowed us to directly compare the M proteins in wild-type and mutant virions using an anti-M monoclonal antibody that recognizes the MHV M-protein ectodomain (40).

Virions of MN8 and the wild type were purified by equilibrium centrifugation on continuous gradients of 20 to 30% iodixanol and collected in multiple fractions that were analyzed for infectivity, viral protein, and genomic RNA (Fig. 5). One readily apparent distinction between the two viruses was that they had markedly different buoyant densities. This difference was confirmed by the nearly identical density profiles of the two gradients shown in

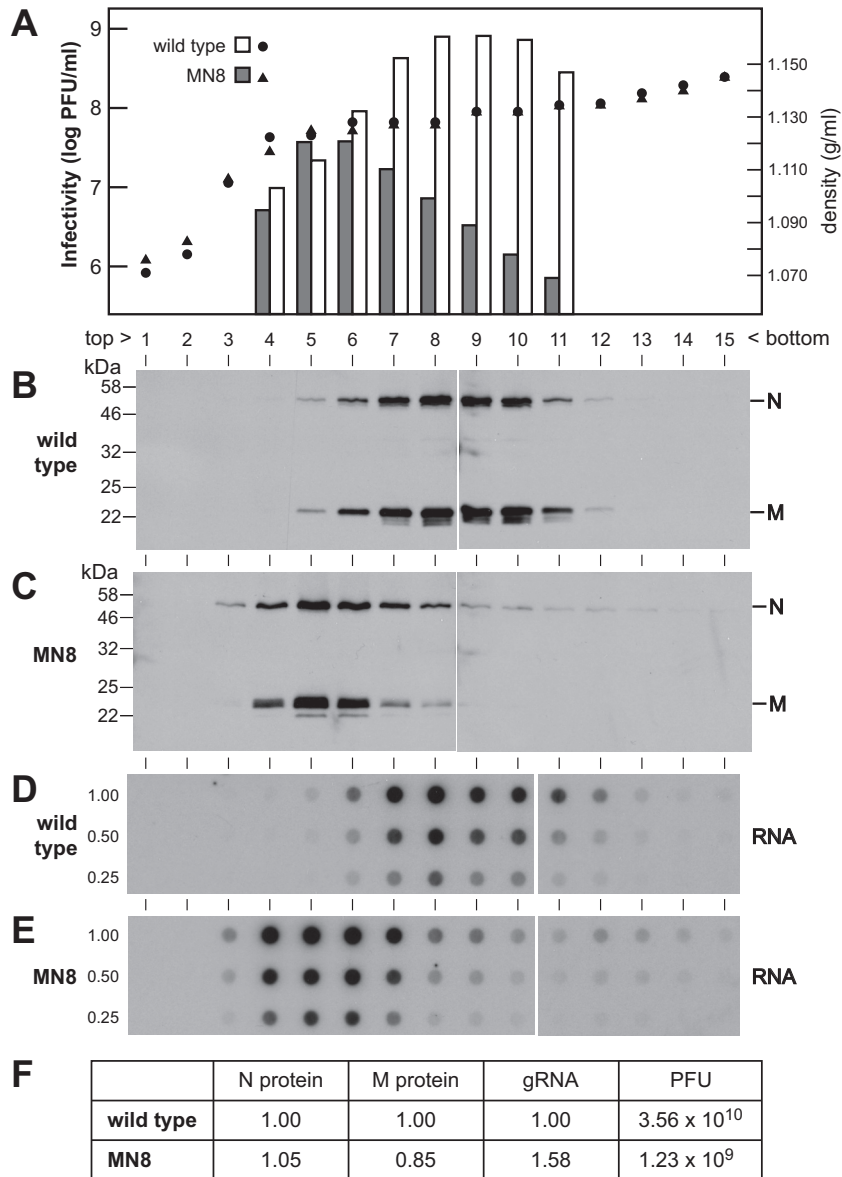


FIG 5 Analysis of MN8 mutant virions. MN8 and wild-type virions were purified by equilibrium centrifugation on continuous gradients of 20 to 30% iodixanol that were collected in 15 fractions, as detailed in Materials and Methods. (A) Infectious titers determined for viral peak fractions 4 through 11 for MN8 (shaded bars) and the wild type (open bars). The densities of all fractions were measured by refractometry (triangles, MN8; circles, wild type). (B, C) Western blots of virion proteins in each fraction probed with polyclonal anti-N (MHV) and monoclonal anti-M ectodomain (MHV) antibodies. (D, E) Northern dot blots of serial 2-fold dilutions of purified virion RNA detected with a probe specific for genomic RNA. (F) Amounts of total protein and genomic RNA (gRNA) and infectivity for wild-type and MN8 virions. Chemiluminescence was quantitated for N protein, M protein, and gRNA and summed over fractions 3 through 12; values are expressed relative to those for the wild type. Total infectivity (numbers of PFU) was summed over fractions 4 through 11.

Fig. 5A. MN8 and wild-type virions were also seen to sediment differently in glycerol-tartrate gradients (41) and in iodixanol gradients of other densities (data not shown). A second salient contrast between the two viruses was that the MN8 mutant had a severely reduced infectious titer, nearly 30-fold lower than that of the wild type (Fig. 5A and F). However, this deficiency was not due to a decreased quantity of assembled viral particles. The levels of N and M proteins detected by Western blotting were comparable for MN8 and wild-type virions, and the two had similar ratios of N protein to M protein (Fig. 5B, C, and F). Additionally, contrary to our original expectations, there was

no impairment in the amount of genomic RNA packaged by the mutant. Indeed, virions of MN8 contained slightly more genomic RNA than wild-type virions (Fig. 5D to F), and Northern blotting verified that MN8 genomic RNA was intact (data not shown). For both the mutant and the wild type, the peaks of protein and RNA coincided with the respective peaks of infectivity. This indicated that MN8 virions did not consist of separate pools of empty and RNA-containing particles.

Surprisingly, MN8 virions contained drastically reduced amounts of S protein compared to wild-type virions. MHV S protein is synthesized as a 180-kDa glycoprotein, S₀, that is cleaved by

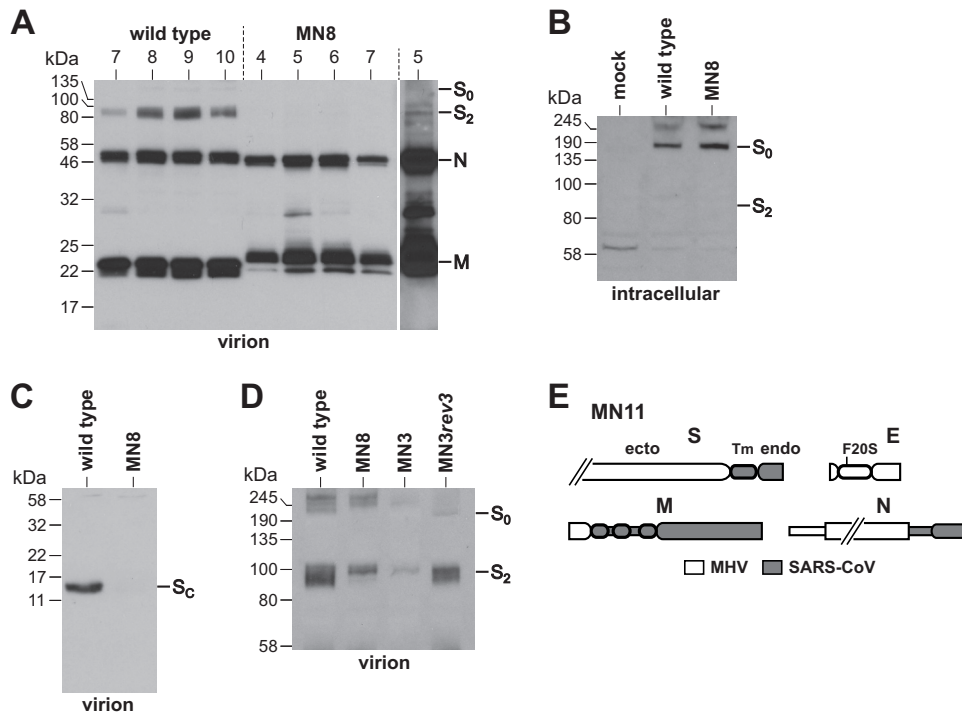


FIG 6 Deficiency of S protein in MN8 virions. (A) Viral peak fractions from iodixanol gradients (fractions 7 to 10 for the wild type and 4 to 7 for MN8) were separated in a 12% SDS-polyacrylamide gel and analyzed by Western blotting by probing with a polyclonal antibody specific for the carboxy terminus of S protein, as well as with polyclonal anti-N and monoclonal anti-M antibodies. At the right is a longer exposure of MN8 fraction 5 to allow visualization of S. (B) Western blot of lysates from mouse 17C11 cells infected with wild-type or MN8 virus, separated in an 8% SDS-polyacrylamide gel, and probed with polyclonal anti-S antibody; mock, uninfected 17C11 cells. (C) Western blot of wild-type and MN8 virions separated in a 15% SDS-polyacrylamide gel and probed with polyclonal anti-S antibody. (D) Western blot of purified wild-type, MN8, MN3, and MN3rev3 virions separated in an 8% SDS-polyacrylamide gel and probed with polyclonal anti-S antibody. S₀, 180-kDa uncleaved S protein; S₂, 90-kDa carboxy-terminal cleavage product of S; S_C, carboxy-terminal fragment of S. (E) Schematic of the lethal substitution in chimera MN11, which did not rescue the S-protein deficiency in MN8.

cellular proteases into amino- and carboxy-terminal halves, S₁ and S₂, respectively. Using an antibody specific for the carboxy terminus of the molecule, we observed that S in wild-type virions was almost entirely in the cleaved S₂ form, although trace amounts of S₀ were seen as well (Fig. 6A). In contrast, only minor quantities of S₂ were detected in MN8 virions. Since S is essential for the initiation of infection, this accounted for the diminished infectivity of the M chimera. This difference in MN8 was not due to a failure to synthesize S. Examination of lysates of infected cells showed that the wild type and MN8 expressed equivalent amounts of S protein, and intracellular S was almost all in the uncleaved S₀ form (Fig. 6B). We also separated virions in a higher-density SDS-polyacrylamide gel to look for evidence of degradation of S protein, analogous to that described for an E-protein mutant of IBV (51). This revealed a minor amount of a 12.5-kDa carboxy-terminal fragment of S protein in wild-type virions, corresponding to roughly 110 amino acids, which would comprise heptad repeat region 2, the Tm domain, and the endodomain (Fig. 6C). However, no such membrane-bound remnant of S was found in MN8 virions, although we would have expected it to be abundant if S had been incorporated into mutant virions and then degraded. Our results therefore indicated that, even though adequate amounts of MHV S protein were available, they were not efficiently incorporated into assembling virions by SARS-CoV M protein. To determine if this was a general characteristic of the SARS-CoV M-protein chimeras, we grew separate stocks of wild-

type, MN8, MN3, and MN3rev3 viruses and purified them on continuous iodixanol gradients. Equivalent quantities of virions, as judged by the N-protein content, were analyzed for S protein. As shown in Fig. 6D, virions of the original chimera, MN3, had an even more severely reduced incorporation of S protein than did those of MN8. In contrast, the large-plaque revertant MN3rev3 had levels of S protein approaching those of the wild type. Thus, the level of S-protein incorporation into various SARS-CoV M-protein chimeras was consistent with their relative titers with respect to the titer of the wild type. To attempt to remedy this defect, we designed an additional chimeric construct, MN11 (Fig. 6E). This mutant incorporated the SARS-CoV S-protein Tm domain and endodomain, in addition to the M, N, and E substitutions already made in MN8. Remarkably, this modification further impaired the virus, since the substitutions in the MN11 construct were lethal. In eight independent targeted RNA recombination trials, no recombinants with MN11 donor RNA were obtained, whereas wild-type control RNA samples in the same experiments yielded robust numbers of recombinants. Contrary to expectations, the inclusion of the SARS-CoV homolog of the region of S protein known to directly interact with the M endodomain was not sufficient to rescue normally assembled viruses. This suggests that there exist structural protein interactions or host cell-specific interactions that remain unaccounted for in coronavirus virion morphogenesis.

DISCUSSION

The construction of interspecies chimeras has proven valuable in the identification of the intra- and intermolecular interactions of the coronavirus N protein (15, 16, 19, 44). We have now applied this approach to the M protein. It was previously found that substitution of the highly homologous BCoV M-protein endodomain had no discernible effect on MHV (40). In the present study, we extended this test over a significantly greater phylogenetic distance, by creating substitutions of the SARS-CoV M sequence in MHV. This has sharpened our picture of the interaction of M with itself and with N protein, and it has revealed unanticipated complexities of the interactions of M with the E and S proteins.

M-N and M-M interactions. Our isolation of the chimera MN3 made clear that incorporation of the heterologous SARS-CoV M protein into MHV required the concomitant inclusion of the SARS-CoV N-protein carboxy-terminal domain N3 (Fig. 2). Chimeras MN1 and MN2, containing just one or the other of these components, were not viable. Moreover, analysis of the chimera MN8 showed that its virions contained abundant amounts of N and M proteins in a ratio comparable to that of wild-type virions (Fig. 5). Together, these results demonstrated that domain N3 is both necessary and sufficient for N protein to interact with M protein in virus assembly. This conclusion conforms to the findings of most previous genetic and molecular biological studies (20–24). The necessity of domain N3 for virion assembly also explains why intracellular carboxy-terminal truncated forms of N protein, likely generated by caspases late in infection (52, 53), are not incorporated into released virions. The sufficiency of N3 accords well with cryo-EM and tomographic reconstructions of MHV and SARS-CoV virions, which found the M endodomain to be connected to the nucleocapsid via a single thread-like connection (54, 55). Nevertheless, some work has purported to detect essential interactions with M that map to parts of N protein other than N3. A mammalian two-hybrid analysis of SARS-CoV N and M localized the interacting segment of N to a region comprising the downstream end of the NTD and all of the SR region (25). Another study used glutathione S-transferase pull-down assays to map the SARS-CoV N-M interaction to a segment of N encompassing the linker between the SR region and the CTD (26). Finally, an analysis of SARS-CoV M and N proteins found the carboxy terminus of N to be required for the formation of virus-like particles with M but proposed an additional M-binding site falling in the center of the NTD (27). The biological relevance of any of these reported interactions remains to be determined, but our results establish that they are not required for virion assembly.

Beyond substitution of the entire SARS-CoV M protein in MHV, we found that it was possible to construct functional chimeric viruses in which intramolecular M-protein substitutions were made (Fig. 4). In the chimera MN8, the ectodomain of MHV M was linked to the Tm domains and endodomain of SARS-CoV M. This substitution mutant was nearly as robust as the complete M-protein chimera MN3. Such an outcome was not unexpected, because the M ectodomain varies considerably among different strains of MHV, and it is relatively tolerant to mutation (40). Additionally, the MHV ectodomain, which is normally O-glycosylated, can be altered to either an unglycosylated or an N-glycosylated form without affecting virus growth in tissue culture (56). Our replacement of the N-glycosylated SARS-CoV M ectodomain with its O-glycosylated MHV M counterpart provides further

support that the mode of M-protein glycosylation is not a crucial factor in virion assembly.

A more extensive intramolecular substitution was made in mutants MN9 and MN10, in which the ectodomain and Tm domains of MHV M were linked to the endodomain of SARS-CoV M (Fig. 4). The viability of these constructs suggests that folding and oligomerization of the M-protein Tm domains and the endodomain, for the most part, occur independently of one another. This conclusion is consistent with our previous finding of truncated endodomain variants of the M protein, designated M*, that evolved by gene duplication in MHV E-deletion mutants to compensate for the absence of E protein (31). Similar M* proteins have also very recently been observed to arise upon passaging of SARS-CoV E-deletion mutants (57). The MHV M* protein was found to be incorporated into purified virions, which showed that interactions among Tm domains were sufficient to sustain the assembly of M* with native M protein. Conversely, cryo-EM analyses of coronavirus virions resolved the basic unit of M to be a dimer, and intermolecular contacts in higher-order oligomers were seen to occur exclusively between M endodomains (30). Thus, the MN9 and MN10 chimeras demonstrate that these two classes of interactions can even be apportioned between M Tm domains and endodomains derived from two divergent coronavirus species.

Although the M protein could be partitioned at domain boundaries, we were not able to further dissect the M endodomain to identify a short linear segment functionally analogous to domain N3 of N protein. Various considerations had indicated that this ought to be possible. First, an early characterization of M protein showed that roughly 15 carboxy-terminal residues were susceptible to protease digestion, which was taken to mean that the carboxy terminus of M was structurally separate from the rest of the globular endodomain (28, 29). Second, prior genetic studies mapped a dominant role in the MHV M-N interaction to an electrostatic bridge between the penultimate M residue, R227, and residues D440 and D441 in domain N3 (20–23). Additionally, *in vitro* assays with TGEV (32) and SARS-CoV (33) M-protein fragments also appeared to localize the N-binding component of M to within 30 residues of the carboxy terminus. However, our multiple attempts to obtain chimeric recombinants in which crossover sites were chosen at distinct motifs near the carboxy terminus of either SARS-CoV or MHV M protein were uniformly unsuccessful (Fig. 4C). This negative result accords well with previous findings that the mutations in several second-site revertants of defective MHV M or N assembly mutants mapped to positions considerably upstream in the M endodomain (20, 21, 23). Moreover, it was pointed out previously that, in many cases, the identical upstream mutation in the M endodomain was independently isolated either as an intragenic suppressor of certain R227 M-protein mutants or as an intergenic suppressor of a D440/D441 N mutant (23). This convergence presents a strong argument that upstream regions of the M endodomain make direct or indirect contributions to the interaction with N protein. Further evidence for a larger participation of the endodomain comes from cryo-EM reconstructions showing that virion M-protein endodomains exist in either a compact form or an extended form, with only the latter making contact with the nucleocapsid (30). This suggests that binding to domain N3 induces a conformational change affecting the entire M endodomain. Since domain N3 is intrinsically disordered (18), we envision that it fits into a surface on the globular M endodomain composed of residues that are discontinuous

in the primary sequence. More detailed exploration of this interaction would benefit greatly from higher-resolution structural information on the M endodomain, which is as yet unavailable.

M-E and M-S interactions. At the outset of this study, we assumed that interactions with MHV E or S would not be affected by the SARS-CoV M-protein substitution. Nevertheless, despite the complete reconstitution of the M-N interaction in chimeric viruses, the transplanted SARS-CoV M protein did not perform well with the other two structural proteins of MHV. In a previous study, we showed that the SARS-CoV E protein could efficiently replace the MHV E protein (38), which seemed to imply that the fitness of the chimera with the reciprocal pairing of MHV E with SARS-CoV M would be equally robust. However, the marked temperature sensitivity of the original M chimera, MN3, was found to be partially suppressed by mutations in the MHV E protein (Fig. 3). Although there is extensive evidence for the colocalization and association of M and E in infected cells (8, 58), this is the first observed instance of genetic cross talk between the M and E proteins. Previously, only intragenic revertants of E mutants were isolated (38, 59–61). This finding suggested that the SARS-CoV M protein would, ideally, require its homologous E partner. Paradoxically, though, substitution of the entire SARS-CoV E protein in mutant MN6 was deleterious, rather than beneficial (Fig. 3).

E protein is known to have at least three separate functions. First, it promotes the assembly of virions, specifically, through mediating aggregation-prone M-M interactions in the membrane of the budding compartment (6). Second, it triggers disassembly of the Golgi compartment, which somehow facilitates the cellular egress of assembled virions (51, 62, 63). Third, E associates with host factors, thereby affecting cell signaling and viral pathogenesis (64, 65). The first two of these functions, virion assembly and Golgi compartment disruption, are carried out by distinct oligomeric states of the E molecule (46). The third role is the only one that has so far been shown to depend on the ion channel activity of E protein (61). Not all functions of E protein appear to be required by all coronaviruses. The consequences of deletion of the E gene were seen to vary from modest impairment for SARS-CoV (66) to severe impairment for MHV (38, 67) and lethality for TGEV and MERS-CoV (68, 69); also, for SARS-CoV, the E-deletion phenotype was dependent on cell type. The multiplicity of roles of E protein likely explains why we were previously able to substitute the phylogenetically distant E proteins of SARS-CoV or IBV for the E protein of MHV but, on the other hand, the TGEV E protein was inert in an MHV background (38). Thus, some functions of E may be interchangeable between a given pair of coronaviruses, while others are not. It is therefore conceivable that transplanting the SARS-CoV M protein into MHV placed it in a heterologous environment where neither MHV E nor SARS-CoV E could simultaneously (i) address the requirements of M protein and (ii) interact with cellular components in a manner optimal for productive infection.

More enigmatic than the M-E interaction was the defective M-S interaction in the SARS-CoV M chimera. Our analysis of the MN8 mutant revealed that virions of the chimera had a striking deficiency of S protein and, consequently, a much higher particle-to-PFU ratio than the wild type (Fig. 6). MN8 virions also had a lower buoyant density than wild-type virions (Fig. 5), which may be attributed to the lack of S or may point to some as yet uncharacterized defect in virion morphogenesis in the chimera. There is

ample evidence that M protein has the sole responsibility for recruiting S protein into virions (9, 10) through interactions that localize to the endodomain of S (41, 42). One possible reason for the reduced complement of S protein in MN8 could be that the SARS-CoV M protein cannot efficiently bind to the MHV S endodomain. This seems unlikely, given that the opposite arrangement is fully functional. Previous work showed that the SARS-CoV S-protein Tm domain and endodomain were completely able to replace their MHV S counterpart (43, 70). Additionally, a foreign membrane protein harboring the SARS-CoV S Tm domain and endodomain was incorporated into MHV virions at a slightly higher efficiency than the MHV version of the same protein (43). Moreover, if the carboxy terminus of MHV S was incompatible with SARS-CoV M, then the defect in the MN8 mutant should have been repaired by substitution of the SARS-CoV S Tm domain and endodomain. Surprisingly, that substitution was lethal in that chimeric construct (MN11).

A second possible cause of the sparse incorporation of S protein into MN8 virions could be that despite being well able to interact, the two proteins colocalize too briefly to do so efficiently. It has been shown that the terminus of the SARS-CoV S endodomain contains a coatamer complex I (COPI)-binding KXHXX motif that is thought to be responsible for recycling of S protein from the Golgi compartment back to the ER, thus increasing the time that S spends in the proximity of M protein (71). The MHV S-protein endodomain does not possess such a signal, although this lack does not impede its ability to interact with the MHV M protein. Again, if this constituted a deficiency in MN8 with respect to S protein contacting the SARS-CoV M protein, then it should have been rescued by the SARS-CoV S endodomain substitution in the MN11 chimera. Finally, we could find no evidence that MHV S protein was incorporated into MN8 virions but subsequently degraded, as was found to happen with a particular E-protein mutant of IBV (51). Thus, further work will be required to unravel the complete range of intermolecular interactions in which the coronavirus M protein participates.

ACKNOWLEDGMENTS

We thank the Applied Genomics Technology and Bioinformatics Core Facilities of the Wadsworth Center for Sanger and next-generation DNA sequencing and genomic sequence analysis. We thank the NIH Biodefense and Emerging Infections Research Resources Repository for providing anti-SARS-CoV M-protein monoclonal antibody.

FUNDING INFORMATION

This work, including the efforts of Paul S. Masters, was funded by HHS | National Institutes of Health (NIH) (R01 AI064603).

The funders had no role in study design, data collection and interpretation, or the decision to submit the work for publication.

REFERENCES

1. Masters PS, Perlman S. 2013. Coronaviridae, p 825–858. *In* Knipe DM, Howley PM, Cohen JL, Griffin DE, Lamb RA, Martin MA, Racaniello VR, Roizman B (ed), *Fields virology*, 6th ed, vol 1. Lippincott Williams & Wilkins, Philadelphia, PA.
2. Perlman S, Netland J. 2009. Coronaviruses post-SARS: update on replication and pathogenesis. *Nat Rev Microbiol* 7:439–450. <http://dx.doi.org/10.1038/nrmicro2147>.
3. Vennema H, Godeke GJ, Rossen JW, Voorhout WF, Horzinek MC, Opstelten DJ, Rottier PJ. 1996. Nucleocapsid-independent assembly of coronavirus-like particles by co-expression of viral envelope protein genes. *EMBO J* 15:2020–2028.

4. Bos EC, Luytjes W, van der Meulen HV, Koerten HK, Spaan WJ. 1996. The production of recombinant infectious D1-particles of a murine coronavirus in the absence of helper virus. *Virology* 218:52–60. <http://dx.doi.org/10.1006/viro.1996.0165>.
5. Corse E, Machamer CE. 2000. Infectious bronchitis virus E protein is targeted to the Golgi complex and directs release of virus-like particles. *J Virol* 74:4319–4326. <http://dx.doi.org/10.1128/JVI.74.9.4319-4326.2000>.
6. Boscarino JA, Logan HL, Lacny JJ, Gallagher TM. 2008. Envelope protein palmitoylations are crucial for murine coronavirus assembly. *J Virol* 82:2989–2999. <http://dx.doi.org/10.1128/JVI.01906-07>.
7. Siu YL, Teoh KT, Lo J, Chan CM, Kien F, Escriu N, Tsao SW, Nicholls JM, Altmeyer R, Peiris JS, Bruzzone R, Nal B. 2008. The M, E, and N structural proteins of the severe acute respiratory syndrome coronavirus are required for efficient assembly, trafficking, and release of virus-like particles. *J Virol* 82:11318–11330. <http://dx.doi.org/10.1128/JVI.01052-08>.
8. Venkatagopalan P, Daskalova SM, Lopez LA, Dolezal KA, Hogue BG. 2015. Coronavirus envelope (E) protein remains at the site of assembly. *Virology* 478:75–85. <http://dx.doi.org/10.1016/j.virol.2015.02.005>.
9. Opstelten DJ, Raamsman MJ, Wolfs K, Horzinek MC, Rottier PJ. 1995. Envelope glycoprotein interactions in coronavirus assembly. *J Cell Biol* 131:339–349. <http://dx.doi.org/10.1083/jcb.131.2.339>.
10. Nguyen VP, Hogue BG. 1997. Protein interactions during coronavirus assembly. *J Virol* 71:9278–9284.
11. Holmes KV, Dollar EW, Sturman LS. 1981. Tunicamycin resistant glycosylation of a coronavirus glycoprotein: demonstration of a novel type of viral glycoprotein. *Virology* 115:334–344. [http://dx.doi.org/10.1016/0042-6822\(81\)90115-X](http://dx.doi.org/10.1016/0042-6822(81)90115-X).
12. Rottier PJM, Horzinek MC, van der Zeijst BAM. 1981. Viral protein synthesis in mouse hepatitis virus strain A59-infected cells: effects of tunicamycin. *J Virol* 40:350–357.
13. Chang CK, Hou MH, Chang CF, Hsiao CD, Huang TH. 2014. The SARS coronavirus nucleocapsid protein—forms and functions. *Antiviral Res* 103:39–50. <http://dx.doi.org/10.1016/j.antiviral.2013.12.009>.
14. Hurst KR, Koetzner CA, Masters PS. 2009. Identification of in vivo-interacting domains of the murine coronavirus nucleocapsid protein. *J Virol* 83:7221–7234. <http://dx.doi.org/10.1128/JVI.00440-09>.
15. Hurst KR, Ye R, Goebel SJ, Jayaraman P, Masters PS. 2010. An interaction between the nucleocapsid protein and a component of the replicase-transcriptase complex is crucial for the infectivity of coronavirus genomic RNA. *J Virol* 84:10276–10288. <http://dx.doi.org/10.1128/JVI.01287-10>.
16. Kuo L, Koetzner CA, Hurst KR, Masters PS. 2014. Recognition of the murine coronavirus genomic RNA packaging signal depends on the second RNA-binding domain of the nucleocapsid protein. *J Virol* 88:4451–4465. <http://dx.doi.org/10.1128/JVI.03866-13>.
17. Chang CK, Chen CM, Chiang MH, Hsu YL, Huang TH. 2013. Transient oligomerization of the SARS-CoV N protein—implication for virus ribonucleoprotein packaging. *PLoS One* 8:e65045. <http://dx.doi.org/10.1371/journal.pone.0065045>.
18. Chang CK, Hsu YL, Chang YH, Chao FA, Wu MC, Huang YS, Hu CK, Huang TH. 2009. Multiple nucleic acid binding sites and intrinsic disorder of severe acute respiratory syndrome coronavirus nucleocapsid protein: implications for ribonucleocapsid protein packaging. *J Virol* 83:2255–2264. <http://dx.doi.org/10.1128/JVI.02001-08>.
19. Hurst KR, Koetzner CA, Masters PS. 2013. Characterization of a critical interaction between the coronavirus nucleocapsid protein and nonstructural protein 3 of the viral replicase-transcriptase complex. *J Virol* 87:9159–9172. <http://dx.doi.org/10.1128/JVI.01275-13>.
20. Kuo L, Masters PS. 2002. Genetic evidence for a structural interaction between the carboxy termini of the membrane and nucleocapsid proteins of mouse hepatitis virus. *J Virol* 76:4987–4999. <http://dx.doi.org/10.1128/JVI.76.10.4987-4999.2002>.
21. Hurst KR, Kuo L, Koetzner CA, Ye R, Hsue B, Masters PS. 2005. A major determinant for membrane protein interaction localizes to the carboxy-terminal domain of the mouse coronavirus nucleocapsid protein. *J Virol* 79:13285–13297. <http://dx.doi.org/10.1128/JVI.79.21.13285-13297.2005>.
22. Verma S, Bednar V, Blount A, Hogue BG. 2006. Identification of functionally important negatively charged residues in the carboxy end of mouse hepatitis coronavirus A59 nucleocapsid protein. *J Virol* 80:4344–4355. <http://dx.doi.org/10.1128/JVI.80.9.4344-4355.2006>.
23. Verma S, Lopez LA, Bednar V, Hogue BG. 2007. Importance of the penultimate positive charge in mouse hepatitis coronavirus A59 membrane protein. *J Virol* 81:5339–5348. <http://dx.doi.org/10.1128/JVI.02427-06>.
24. Luo H, Wu D, Shen C, Chen K, Shen X, Jiang H. 2006. Severe acute respiratory syndrome coronavirus membrane protein interacts with nucleocapsid protein mostly through their carboxyl termini by electrostatic attraction. *Int J Biochem Cell Biol* 38:589–599. <http://dx.doi.org/10.1016/j.biocel.2005.10.022>.
25. He R, Leeson A, Ballantine M, Andonov A, Baker L, Dobie F, Li Y, Bastien N, Feldmann H, Strocher U, Theriault S, Cutts T, Cao J, Booth TF, Plummer FA, Tyler S, Li X. 2004. Characterization of protein-protein interactions between the nucleocapsid protein and membrane protein of the SARS coronavirus. *Virus Res* 105:121–125. <http://dx.doi.org/10.1016/j.virusres.2004.05.002>.
26. Fang X, Ye LB, Zhang Y, Li B, Li S, Kong L, Wang Y, Zheng H, Wang W, Wu Z. 2006. Nucleocapsid amino acids 211 to 254, in particular, tetrad glutamines, are essential for the interaction between the nucleocapsid and membrane proteins of SARS-associated coronavirus. *J Microbiol* 44:577–580.
27. Hatakeyama S, Matsuoka Y, Ueshiba H, Komatsu N, Itoh K, Shichijo S, Kanai T, Fukushi M, Ishida I, Kirikae T, Sasazuki T, Miyoshi-Akiyama T. 2008. Dissection and identification of regions required to form pseudoparticles by the interaction between the nucleocapsid (N) and membrane (M) proteins of SARS coronavirus. *Virology* 380:99–108. <http://dx.doi.org/10.1016/j.virol.2008.07.012>.
28. Rottier P, Brandenburg D, Armstrong J, van der Zeijst B, Warren G. 1984. Assembly in vitro of a spanning membrane protein of the endoplasmic reticulum: the E1 glycoprotein of coronavirus mouse hepatitis virus A59. *Proc Natl Acad Sci U S A* 81:1421–1425. <http://dx.doi.org/10.1073/pnas.81.5.1421>.
29. Rottier PJ, Welling GW, Welling-Wester S, Niesters HG, Lenstra JA, Van der Zeijst BA. 1986. Predicted membrane topology of the coronavirus protein E1. *Biochemistry* 25:1335–1339. <http://dx.doi.org/10.1021/bi00354a022>.
30. Neuman BW, Kiss G, Kunding AH, Bhella D, Baksh MF, Connelly S, Droese B, Klaus JP, Makino S, Sawicki SG, Siddell SG, Stamou DG, Wilson IA, Kuhn P, Buchmeier MJ. 2011. A structural analysis of M protein in coronavirus assembly and morphology. *J Struct Biol* 174:11–22. <http://dx.doi.org/10.1016/j.jsb.2010.11.021>.
31. Kuo L, Masters PS. 2010. Evolved variants of the membrane protein can partially replace the envelope protein in murine coronavirus assembly. *J Virol* 84:12872–12885. <http://dx.doi.org/10.1128/JVI.01850-10>.
32. Escors D, Ortego J, Laude H, Enjuanes L. 2001. The membrane M protein carboxy terminus binds to transmissible gastroenteritis coronavirus core and contributes to core stability. *J Virol* 75:1312–1324. <http://dx.doi.org/10.1128/JVI.75.3.1312-1324.2001>.
33. Fang X, Ye L, Timani KA, Li S, Zen Y, Zhao M, Zheng H, Wu Z. 2005. Peptide domain involved in the interaction between membrane protein and nucleocapsid protein of SARS-associated coronavirus. *J Biochem Mol Biol* 38:381–385. <http://dx.doi.org/10.5483/BMBRep.2005.38.4.381>.
34. de Haan CA, Smeets M, Vernooij F, Vennema H, Rottier PJ. 1999. Mapping of the coronavirus membrane protein domains involved in interaction with the spike protein. *J Virol* 73:7441–7452.
35. McBride CE, Machamer CE. 2010. A single tyrosine in the severe acute respiratory syndrome coronavirus membrane protein cytoplasmic tail is important for efficient interaction with spike protein. *J Virol* 84:1891–1901. <http://dx.doi.org/10.1128/JVI.02458-09>.
36. Goebel SJ, Hsue B, Dombrowski TF, Masters PS. 2004. Characterization of the RNA components of a putative molecular switch in the 3′ untranslated region of the murine coronavirus genome. *J Virol* 78:669–682. <http://dx.doi.org/10.1128/JVI.78.2.669-682.2004>.
37. Kuo L, Godeke GJ, Raamsman MJ, Masters PS, Rottier PJ. 2000. Retargeting of coronavirus by substitution of the spike glycoprotein ectodomain: crossing the host cell species barrier. *J Virol* 74:1393–1406. <http://dx.doi.org/10.1128/JVI.74.3.1393-1406.2000>.
38. Kuo L, Hurst KR, Masters PS. 2007. Exceptional flexibility in the sequence requirements for coronavirus small envelope protein function. *J Virol* 81:2249–2262. <http://dx.doi.org/10.1128/JVI.01577-06>.
39. Tripp RA, Haynes LM, Moore D, Anderson B, Tamin A, Harcourt BH, Jones LP, Yilla M, Babcock GJ, Greenough T, Ambrosino DM, Alvarez R, Callaway J, Cavitt S, Kamrud K, Alterson H, Smith J, Harcourt JL, Miao C, Razdan R, Comer JA, Rollin PE, Ksiazek TG, Sanchez A, Rota PA, Bellini WJ, Anderson LJ. 2005. Monoclonal antibodies to SARS-

- associated coronavirus (SARS-CoV): identification of neutralizing and antibodies reactive to S, N, M and E viral proteins. *J Virol Methods* 128: 21–28. <http://dx.doi.org/10.1016/j.jviromet.2005.03.021>.
40. de Haan CA, Kuo L, Masters PS, Vennema H, Rottier PJ. 1998. Coronavirus particle assembly: primary structure requirements of the membrane protein. *J Virol* 72:6838–6850.
 41. Ye R, Montalto-Morrison C, Masters PS. 2004. Genetic analysis of determinants for spike glycoprotein assembly into murine coronavirus virions: distinct roles for charge-rich and cysteine-rich regions of the endodomain. *J Virol* 78:9904–9917. <http://dx.doi.org/10.1128/JVI.78.18.9904-9917.2004>.
 42. Bosch BJ, de Haan CA, Smits SL, Rottier PJ. 2005. Spike protein assembly into the coronavirus: exploring the limits of its sequence requirements. *Virology* 334:306–318. <http://dx.doi.org/10.1016/j.virol.2005.02.001>.
 43. Yao Q, Masters PS, Ye R. 2013. Negatively charged residues in the endodomain are critical for specific assembly of spike protein into murine coronavirus. *Virology* 442:74–81. <http://dx.doi.org/10.1016/j.virol.2013.04.001>.
 44. Peng D, Koetzner CA, McMahon T, Zhu Y, Masters PS. 1995. Construction of murine coronavirus mutants containing interspecies chimeric nucleocapsid proteins. *J Virol* 69:5475–5484.
 45. Koetzner CA, Parker MM, Ricard CS, Sturman LS, Masters PS. 1992. Repair and mutagenesis of the genome of a deletion mutant of the coronavirus mouse hepatitis virus by targeted RNA recombination. *J Virol* 66:1841–1848.
 46. Westerbeck JW, Machamer CE. 2015. A coronavirus E protein is present in two distinct pools with different effects on assembly and the secretory pathway. *J Virol* 89:9313–9323. <http://dx.doi.org/10.1128/JVI.01237-15>.
 47. de Haan CA, Vennema H, Rottier PJ. 2000. Assembly of the coronavirus envelope: homotypic interactions between the M proteins. *J Virol* 74: 4967–4978. <http://dx.doi.org/10.1128/JVI.74.11.4967-4978.2000>.
 48. Arndt AL, Larson BJ, Hogue BG. 2010. A conserved domain in the coronavirus membrane protein tail is important for virus assembly. *J Virol* 84:11418–11428. <http://dx.doi.org/10.1128/JVI.01131-10>.
 49. Niemann H, Geyer R, Klenk HD, Linder D, Stirn S, Wirth M. 1984. The carbohydrates of mouse hepatitis virus (MHV) A59: structures of the O-glycosidically linked oligosaccharides of glycoprotein E1. *EMBO J* 3:665–670.
 50. Oostra M, de Haan CA, de Groot RJ, Rottier PJ. 2006. Glycosylation of the severe acute respiratory syndrome coronavirus triple-spanning membrane proteins 3a and M. *J Virol* 80:2326–2336. <http://dx.doi.org/10.1128/JVI.80.5.2326-2336.2006>.
 51. Machamer CE, Youn S. 2006. The transmembrane domain of the infectious bronchitis virus E protein is required for efficient virus release. *Adv Exp Med Biol* 581:193–198. http://dx.doi.org/10.1007/978-0-387-33012-9_33.
 52. Eléouët JF, Slee EA, Saurini F, Castagné N, Poncet D, Garrido C, Solary E, Martin SJ. 2000. The viral nucleocapsid protein of transmissible gastroenteritis coronavirus (TGEV) is cleaved by caspase-6 and -7 during TGEV-induced apoptosis. *J Virol* 74:3975–3983. <http://dx.doi.org/10.1128/JVI.74.9.3975-3983.2000>.
 53. Diemer C, Schneider M, Seebach J, Quaas J, Frösner G, Schätzl HM, Gilch S. 2008. Cell type-specific cleavage of nucleocapsid protein by effector caspases during SARS coronavirus infection. *J Mol Biol* 376:23–34. <http://dx.doi.org/10.1016/j.jmb.2007.11.081>.
 54. Neuman BW, Adair BD, Yoshioka C, Quispe JD, Orca G, Kuhn P, Milligan RA, Yeager M, Buchmeier MJ. 2006. Supramolecular architecture of severe acute respiratory syndrome coronavirus revealed by electron cryomicroscopy. *J Virol* 80:7918–7928. <http://dx.doi.org/10.1128/JVI.00645-06>.
 55. Bárcena M, Oostergetel GT, Bartelink W, Faas FG, Verkley A, Rottier PJ, Koster AJ, Bosch BJ. 2009. Cryo-electron tomography of mouse hepatitis virus: insights into the structure of the coronavirus. *Proc Natl Acad Sci U S A* 106:582–587. <http://dx.doi.org/10.1073/pnas.0805270106>.
 56. de Haan CA, de Wit M, Kuo L, Montalto-Morrison C, Haagmans BL, Weiss SR, Masters PS, Rottier PJ. 2003. The glycosylation status of the murine hepatitis coronavirus M protein affects the interferogenic capacity of the virus in vitro and its ability to replicate in the liver but not the brain. *Virology* 312:395–406. [http://dx.doi.org/10.1016/S0042-6822\(03\)00235-6](http://dx.doi.org/10.1016/S0042-6822(03)00235-6).
 57. Jimenez-Guardeño JM, Regla-Nava JA, Nieto-Torres JL, DeDiego ML, Castaño-Rodríguez C, Fernández-Delgado R, Perlman S, Enjuanes L. 2015. Identification of the mechanisms causing reversion to virulence in an attenuated SARS-CoV for the design of a genetically stable vaccine. *PLoS Pathog* 11:e1005215. <http://dx.doi.org/10.1371/journal.ppat.1005215>.
 58. Corse E, Machamer CE. 2003. The cytoplasmic tails of infectious bronchitis virus E and M proteins mediate their interaction. *Virology* 312:25–34. [http://dx.doi.org/10.1016/S0042-6822\(03\)00175-2](http://dx.doi.org/10.1016/S0042-6822(03)00175-2).
 59. Fischer F, Stegen CF, Masters PS, Samsonoff WA. 1998. Analysis of constructed E gene mutants of mouse hepatitis virus confirms a pivotal role for E protein in coronavirus assembly. *J Virol* 72:7885–7894.
 60. Ye Y, Hogue BG. 2007. Role of the coronavirus E viroporin protein transmembrane domain in virus assembly. *J Virol* 81:3597–3607. <http://dx.doi.org/10.1128/JVI.01472-06>.
 61. Nieto-Torres JL, DeDiego ML, Verdía-Báguena C, Jimenez-Guardeño JM, Regla-Nava JA, Fernández-Delgado R, Castaño-Rodríguez C, Alcaraz A, Torres J, Aguilera VM, Enjuanes L. 2014. Severe acute respiratory syndrome coronavirus envelope protein ion channel activity promotes virus fitness and pathogenesis. *PLoS Pathog* 10:e1004077. <http://dx.doi.org/10.1371/journal.ppat.1004077>.
 62. Ruch TR, Machamer CE. 2011. The hydrophobic domain of infectious bronchitis virus E protein alters the host secretory pathway and is important for release of infectious virus. *J Virol* 85:675–685. <http://dx.doi.org/10.1128/JVI.01570-10>.
 63. Ruch TR, Machamer CE. 2012. A single polar residue and distinct membrane topologies impact the function of the infectious bronchitis coronavirus E protein. *PLoS Pathog* 8:e1002674. <http://dx.doi.org/10.1371/journal.ppat.1002674>.
 64. Teoh KT, Siu YL, Chan WL, Schlüter MA, Liu CJ, Peiris JS, Bruzzone R, Margolis B, Nal B. 2010. The SARS coronavirus E protein interacts with PALS1 and alters tight junction formation and epithelial morphogenesis. *Mol Biol Cell* 21:3838–3852. <http://dx.doi.org/10.1091/mbc.E10-04-0338>.
 65. Jimenez-Guardeño JM, Nieto-Torres JL, DeDiego ML, Regla-Nava JA, Fernández-Delgado R, Castaño-Rodríguez C, Enjuanes L. 2014. The PDZ-binding motif of severe acute respiratory syndrome coronavirus envelope protein is a determinant of viral pathogenesis. *PLoS Pathog* 10:e1004320. <http://dx.doi.org/10.1371/journal.ppat.1004320>.
 66. DeDiego ML, Alvarez E, Almazán F, Rejas MT, Lamirande E, Roberts A, Shieh WJ, Zaki SR, Subbarao K, Enjuanes L. 2007. A severe acute respiratory syndrome coronavirus that lacks the E gene is attenuated in vitro and in vivo. *J Virol* 81:1701–1713. <http://dx.doi.org/10.1128/JVI.01467-06>.
 67. Kuo L, Masters PS. 2003. The small envelope protein E is not essential for murine coronavirus replication. *J Virol* 77:4597–4608. <http://dx.doi.org/10.1128/JVI.77.8.4597-4608.2003>.
 68. Ortego J, Ceriani JE, Patiño C, Plana J, Enjuanes L. 2007. Absence of E protein arrests transmissible gastroenteritis coronavirus maturation in the secretory pathway. *Virology* 36:296–308.
 69. Almazán F, DeDiego ML, Sola I, Zuñiga S, Nieto-Torres JL, Marquez-Jurado S, Andrés G, Enjuanes L. 2013. Engineering a replication-competent, propagation-defective Middle East respiratory syndrome coronavirus as a vaccine candidate. *mBio* 4:e00650-13. <http://dx.doi.org/10.1128/mBio.00650-13>.
 70. Lokugamage KG, Yoshikawa-Iwata N, Ito N, Watts DM, Wyde PR, Wang N, Newman P, Kent Tseng CT, Peters CJ, Makino S. 2008. Chimeric coronavirus-like particles carrying severe acute respiratory syndrome coronavirus (SCoV) S protein protect mice against challenge with SCoV. *Vaccine* 26:797–808. <http://dx.doi.org/10.1016/j.vaccine.2007.11.092>.
 71. McBride CE, Li J, Machamer CE. 2007. The cytoplasmic tail of the severe acute respiratory syndrome coronavirus spike protein contains a novel endoplasmic reticulum retrieval signal that binds COPI and promotes interaction with membrane protein. *J Virol* 81:2418–2428. <http://dx.doi.org/10.1128/JVI.02146-06>.